Synthesis and Characterization of Bromine- and Hydroxyl-Functionalized Polyaminals for CO_2 Capture

Maha M. Alotaibi , Abeer M. Alharthi , Nazeeha S. Alkayal * , Maymounah A. Alrayyani

Posted Date: 25 December 2023

doi: 10.20944/preprints202312.1792.v1

Keywords: porous organic polymer, polyaminal-linked polymers, melamine, surface area, CO2 capture

Article

Synthesis and Characterization of Bromine- and Hydroxyl-Functionalized Polyaminals for CO_2 Capture

Maha M. Alotaibi, Abeer M. Alharthi, Nazeeha S. Alkayal * and Maymounah A. Alrayyani

Chemistry Department, Faculty of Science, King Abdulaziz University, P.O. Box 80203, Jeddah 21589, Saudi Arabia; mmsalotaibi@kau.edu.sa (M.M.A.); amuidhalharthi@stu.kau.edu.sa (A.M.A.); malrayyani@kau.edu.sa (M.A.A.)

* Correspondence: nalkayal@kau.edu.sa

Abstract: Increased CO_2 emissions and air pollution impact the environment and human health. In this manner, new functionalized polyaminal-based polymers are synthesized via a one-pot polycondensation reaction of melamine with aldehyde monomers 2-bromo-1-naphthaldehyde and 2-hydroxy-1-naphthaldehyde to yield bromine- hydroxyl- functionalized polymer networks PAN-BrNA and PAN-HNA, respectively. The polyaminals porosity parameters were investigated and applied as an adsorbent for CO_2 capture. FTIR, solid-state ^{13}C NMR, and X-ray diffraction verified the PANs structure development. A scanning electron microscope and N_2 adsorption-desorption methods were utilized to identify the porous properties of the polymers at 77 K. The Brunauer-Emmett-Teller (BET) surface area of PAN-BrNA and PAN-HNA is (16.6990 m^2/g) and (716.7568 m^2/g), respectively. At 273 K, PAN-BrNA and PAN-HNA can take CO_2 gas up to (4.42786 cm^3/g) and (47.55 cm^3/g), respectively. The findings show that inserting functional groups has a significant impact on surface area and porosity parameters, as well as CO_2 uptake.

Keywords: porous organic polymer; polyaminal-linked polymers; melamine; surface area; CO_2 capture

1. Introduction

Developing innovative and environmentally friendly approaches to meet rising energy and fuel consumption has generated interest, owing to limited supplies of fossil fuels, a remarkable increase in carbon dioxide levels, and worrying concerns regarding global warming [1]. The scientific community is concerned with how to effectively achieve CO_2 capture and storage, which has resulted in significant interest in creating new functional materials along with technologies to deal with this concern on a global scale, including metal-organic frameworks (MOFs) [2], activated carbon [3], zeolites [4], and porous organic polymers (POPs) [5]. Due to the high porosity and tunability of their pore surface functionality, adsorption with POPs is among the most energy-efficient and technically viable methods for capturing CO_2 [6, 7]. Melamine has been used to produce hyper-cross-linked polyaminal networks (PANs) effectively. The produced intermediate imine bond (–C=N–) interacts with the active amino group to form a stable aminal linkage (–NH–CH–NH–) [8]. The addition of nitrogen atoms has previously been shown to improve CO_2 attraction among different gases [6]. The introduction of functional groups into POP networks has demonstrated their effectiveness in terms of surface area, porous characteristics, and CO_2 capture in several reported research studies [9, 10]. Guiyang Li and colleagues created (PAN-P), (PAN-MP), (PAN-FP), and (PAN-FMP). Fluorinated polymers have higher BET-specific surface areas than non-fluorinated polymers, ranging from 615 to 907 $m^2\ g^{-1}$. Furthermore, methyl and trifluoromethyl inclusion on the phenyl rings can efficiently adjust the pore diameters from 0.9 to 0.6 nm. The polar C–F bond and nitrogen-rich polyaminal skeleton result in up to 14.6 wt% CO_2 adsorption [8]. Carboxyl-, hydroxyl-, and nitro-functionalized porous polyaminals (PAN-CP), (PAN-HP), and (PAN-NP) were introduced by Zhang *et al*. PAN-CP and PAN-HP have higher BET surface areas and total pore volumes than the unsubstituted polymer

 doi:10.20944/preprints202312.1792.v1

PAN-P. PAN-CP and PAN-HP demonstrate greater CO_2 uptake of up to 13.3 and 13.5 wt%, respectively, compared to unfunctionalized PAN-P, which has a CO_2 uptake of 11.1 wt% [11]. According to previous research, introducing functional groups alters the surface area and porosity structure and influences CO_2 capture. In this work, 2-bromo-1-naphthaldehyde and 2-hydroxy-1-naphthaldehyde polymerize with melamine to generate (PAN-BrNA) and (PAN-HNA), respectively, using a direct one-step polymerization approach without the utilization of a catalyst, as illustrated in Scheme 1. CO_2 capture was also used to evaluate the adsorption capability of the produced functionalized polymers. The synthesized polymers PAN-BrNA and PAN-HNA composition was investigated using Fourier transform infrared spectroscopy (FTIR), solid-state ^{13}C NMR, X-ray diffraction, and thermogravimetric analysis. Scanning electron microscopes with an energy-dispersive X-ray spectrometer was used to evaluate morphology and elemental analyses. The porosity characteristics of the polymers have been investigated using the physical sorption of nitrogen at 77 K. The polyaminal networks are applied for CO_2 capture.

2. Experimental section

2.1. Materials

2-Bromo-1-naphthaldehyde (97.22%) and 2-Hydroxy-1-naphthaldehyde (98.99%) were purchased from Baoji Guokang Bio-Technology Co., Lt, Baoji City, Mainland China; melamine (97.5%) and dimethyl sulfoxide (DMSO 99%) were purchased from BDH Laboratory Reagents, England, UK; tetrahydrofuran (THF ≥ 99.5%) was purchased from Honeywell, Germany; dichloromethane (≥ 99.8%) supplied from Fisher Chemicals, England; acetone was supplied from Cornaredo (Milano), Italy. All materials were provided commercially and used without further purification.

2.2. Synthesis of functionalized bromine-naphthalene-based polyaminal networks (PAN-BrNA)

A two evacuation-argon-backfill cycle was used for degassing a dry three-necked flask with a stirrer and a condenser. Under argon flow, melamine (0.5 g, 3.96 mmol), 2-bromo-1-naphthaldehyde (0.8 g, 3.40 mmol), and (25 mL) of DMSO were added and heated at 175 °C for 72 hours. After one hour of cooling at room temperature, the product was washed repeatedly with dichloromethane, tetrahydrofuran, and acetone. The dark brown solid that resulted was dried in a vacuum to yield (92.15%).

2.3. Synthesis of functionalized hydroxyl-naphthalene-based polyaminal networks (PAN-HNA)

The synthesis of PAN-HNA was carried out using the same procedure as PAN-BrNA. Melamine (1 g, 7.92 mmol) and 2-hydroxy-1-naphthaldehyde (1.6 g, 9.29 mmol) were reacted in DMSO (50 mL) at 175 °C for 72 h. The produced light brown solid gives a yield (39.6%).

2.4. Instrumentation

The KBr disk approach was used on a Perkin-Elmer FTIR spectrometer to conduct Fourier-transform infrared spectroscopy (FTIR). A Bruker AVANCE I HD 500 MHz spectrophotometer was employed to record solid-state ^{13}C NMR spectra. X-ray diffraction (XRD) evaluations were recorded with a Bruker D8 Advance and Cu Kα at diffraction angles ranging from 10° to 80°. For sample morphology determination, scanning electron microscopy (SEM) analysis was performed on JSM-IT500HR via (JEOL Japan) equipped with an energy-dispersive X-ray spectrometer (EDS) to estimate elemental analysis. Thermogravimetric analysis (TGA) was conducted using a TGA4724 with an increase of temperature of 10 °C min^{-1} in an N_2 atmosphere. N_2 adsorption and desorption measurements were carried out on a Micromeritics 3 Flex 3500. The Langmuir and Brunauer-Emmett-Teller (BET) approaches were used to calculate the material surface area. The t-plot was used to calculate the micropore surface area. Before being analyzed, the sample was degassed at 120 °C for

Preprints (www.preprints.org) | NOT PEER-REVIEWED | Posted: 25 December 2023 doi:10.20944/preprints202312.1792.v1

12 hours under vacuum. Non-local density functional theory (NLDFT) was used to investigate the sample pore size distribution (PSD).

3. Results and discussion

3.1. Synthesis and Characterization

PAN-BrNA and PAN-HNA polymers have dark and light brown powder, respectively, are insoluble in water, and have been tested for stability in various organic solvents such as dimethyl sulfoxide, tetrahydrofuran, and dichloromethane. As illustrated in Scheme 1, the PANs were synthesized utilizing a one-step polycondensation procedure at 175 °C and under an Ar atmosphere to produce hyper-cross-linked polymers.

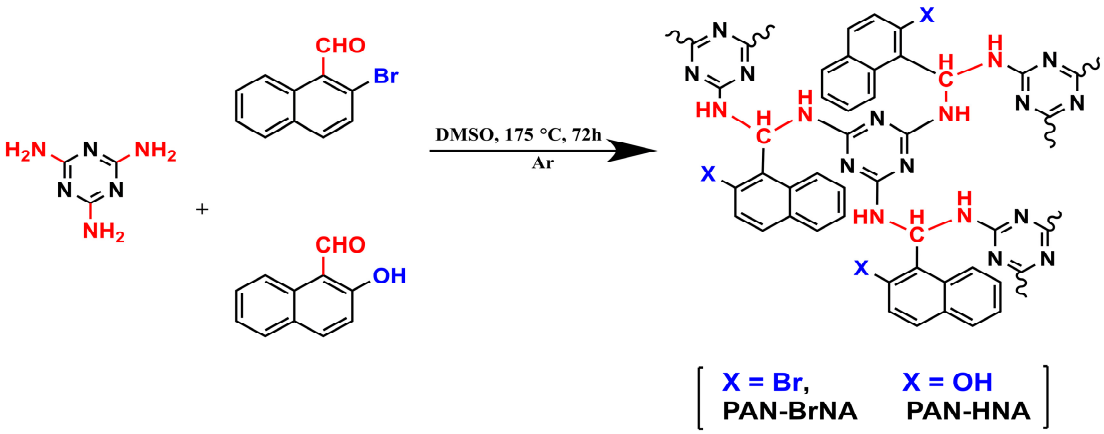

Scheme 1. Synthesis of PAN-BrNA and PAN-HNA.

FTIR analysis investigated the chemical structure and functional groups of raw materials and polymers, as depicted in Figure 1. Melamine has bands associated with the NH_2 stretching frequency at 3470 cm^{-1} and 3420 cm^{-1}. The spectra revealed that the C–O stretching of the carbonyl group of aldehyde monomers at 1678 cm^{-1} and 1622 cm^{-1}, respectively, disappeared in the polymer structure, indicating that the aldehyde group of monomers and melamine in polymer networks were transformed entirely [1]. Triazine rings, characteristic bands of PAN-BrNA, appeared at 1513 and 1404 cm^{-1} in Figure 1 (a), and similar bands at 1541 and 1472 cm^{-1} appeared in Figure 1 (b) attributed to the triazine stretching vibrations for PAN-HNA. The characteristic peaks of C–N exist at 1329 and 1348 cm^{-1} for PAN-BrNA and PAN-HNA, respectively. PAN-BrNA and PAN-HNA have C–H stretching vibrations at 2929 and 2969 cm^{-1}, respectively [12]. For PAN-BrNA, The aminal linkage stretching vibration occurs at 3440 and 1197 cm^{-1}, and the band at 1046 cm^{-1} is due to the stretching vibrations of the C–Br bond [13]. The O–H characteristic peaks are energetically overlapped with N–H, resulting in one broad peak of 3414 cm^{-1} in PAN-HNA spectra [12].

Preprints (www.preprints.org) | NOT PEER-REVIEWED | Posted: 25 December 2023 doi:10.20944/preprints202312.1792.v1

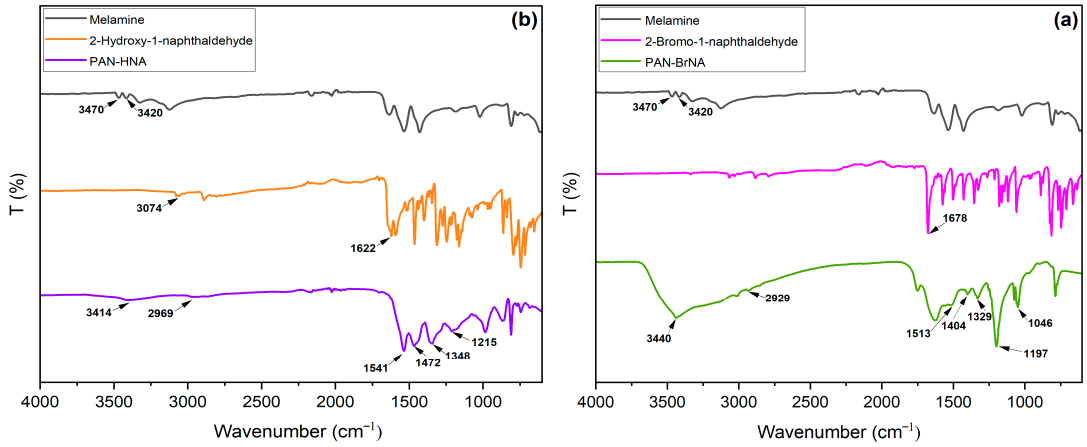

Figure 1. FTIR spectra of (a) melamine, 2-bromo-1-naphthaldehyde, and PAN-BrNA, (b) melamine, 2-hydroxy-1-naphthaldehyde, and PAN-HNA.

In order to further verify the PAN-BrNA and PAN-HNA network structure, the solid-state ^{13}C NMR spectrums were recorded, as shown in Figure 2 (a, b), respectively. The spectrum of PAN-BrNA exhibits triazine ring resonance at 166 ppm. A strong signal appeared at 158 ppm related to the triazine ring carbons attached to the aminal linkage (–NH–CH–NH–). Furthermore, the benzene ring aromatic carbon shows a resonance at 130 ppm. The chemical shift revealed at 50 ppm is related to the aminal linkage formation [14, 15]. The appearance of a signal at 41.5 ppm is assigned to the presence of solvent DMSO. For PAN-HNA, a characteristic carbon triazine ring signal appeared at 167.7 ppm. The resonance that appeared at 153.8 ppm is attributed to the aromatic carbon of the phenolic hydroxyl group. The chemical shift at 131 ppm can be assigned to the carbon signal from benzene rings. Moreover, the broad peak centered at 57.6 ppm is given to the methylene group originating in aminal linkage [16]. Previous research has shown that DMSO decomposes at high temperatures, resulting in the formation of formaldehyde. The condensation interaction with the free amino groups of melamine results in an ether linkage and methylol groups. As a result, a signal appeared at 69.1 and 74.5 ppm associated with the presence of methylol groups and methylene groups in ether linkage, respectively. Furthermore, the signal at 15.7 ppm is related to the C–S group of DMSO [17].

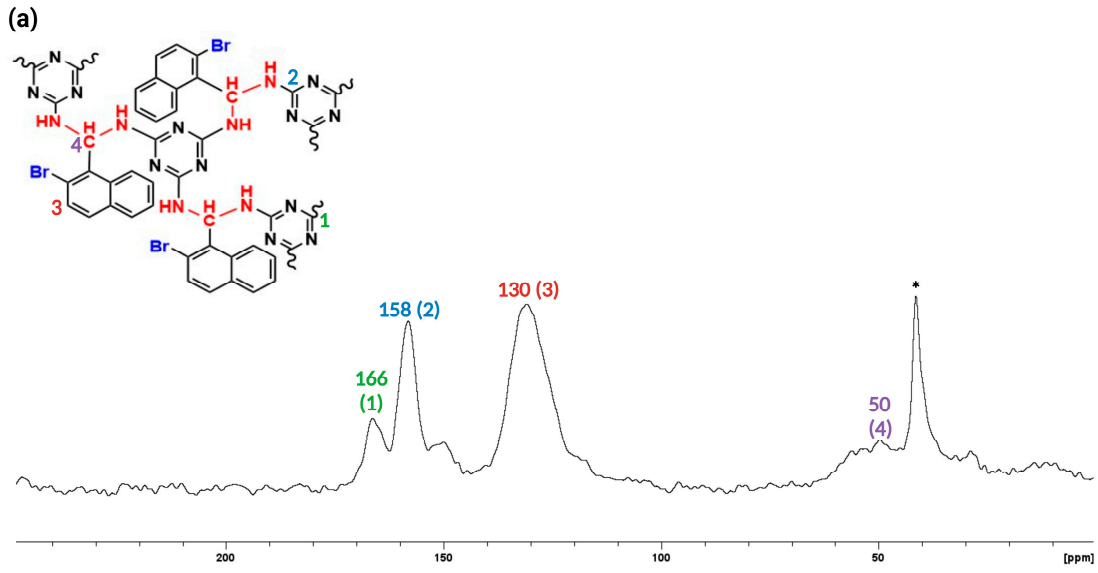

Preprints (www.preprints.org) | NOT PEER-REVIEWED | Posted: 25 December 2023 doi:10.20944/preprints202312.1792.v1

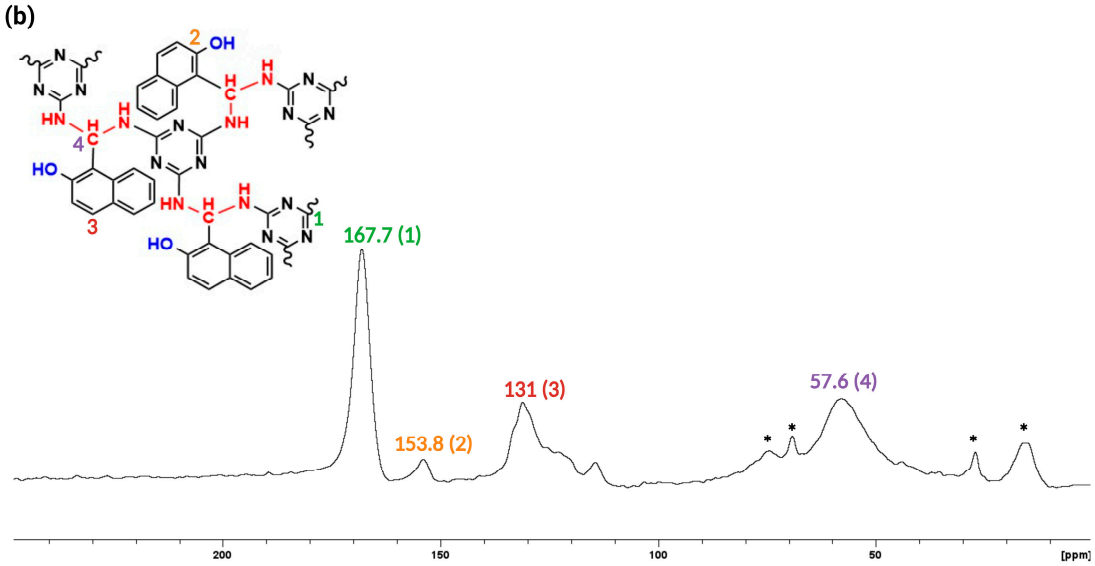

Figure 2. Solid-state ^{13}C NMR spectrum of (a) PAN-BrNA and (b) PAN-HNA.

The occurrence of distinct broad peaks around the region of 2θ = 20° verified the disordered amorphous character of both PAN-BrNA and PAN-HNA in the XRD pattern, as shown in Figure 3 (a, b) [18].

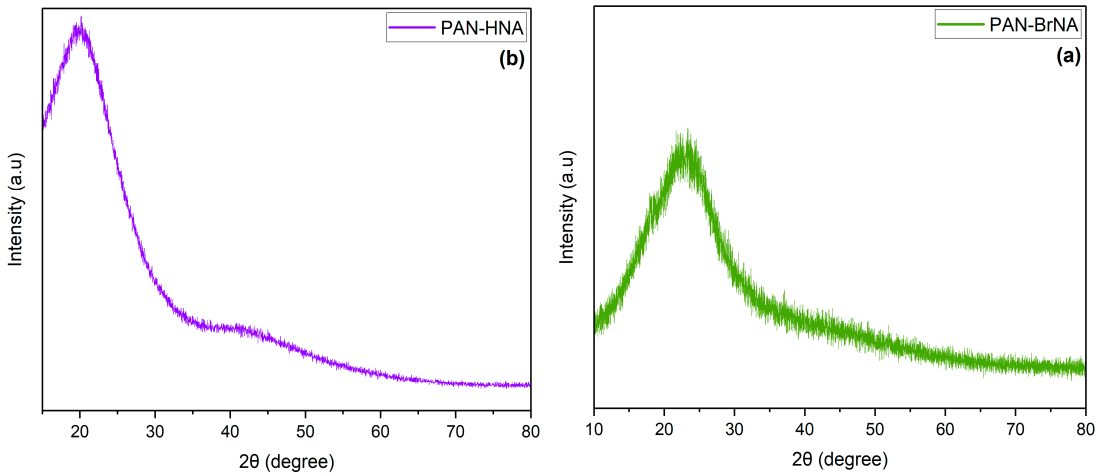

Figure 3. XRD pattern of (a) PAN-BrNA and (b) PAN-HNA.

A scanning electron microscope (SEM) was used to study the morphology of the synthesized PANs. The polyaminals lack the usual spherical morphology of porous polymers, and agglomerated shapes appeared in the images, as shown in Figure 4 (a, b), similar to those found in earlier reported melamine-based porous polymers [19]. The EDX analysis, as depicted in Figure 4 (c, d), confirms the synthesis of PAN-BrNA and PAN-HNA, respectively. The elemental analysis showed that PAN-BrNA consists of (39.19%) carbon, (29.13%) nitrogen, (22.65%) oxygen, and bromine (9.02%). Moreover, PAN-HNA contains (52.50%) carbon, (29.23%) nitrogen, and (18.26%) oxygen, indicating the production of both polyaminals networks.

Preprints (www.preprints.org) | NOT PEER-REVIEWED | Posted: 25 December 2023 doi:10.20944/preprints202312.1792.v1

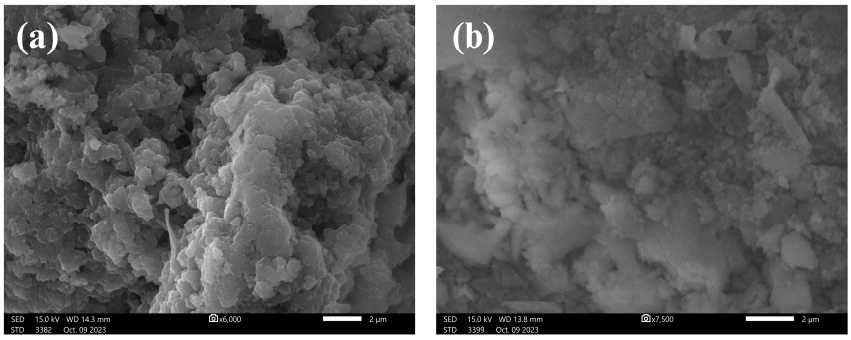

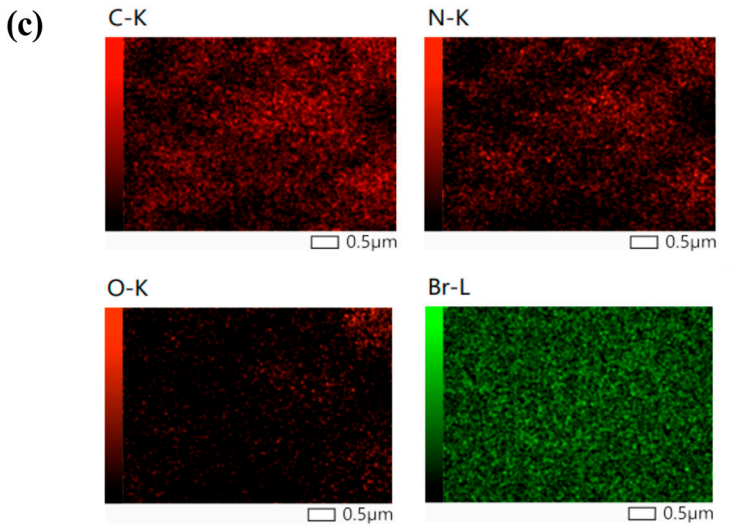

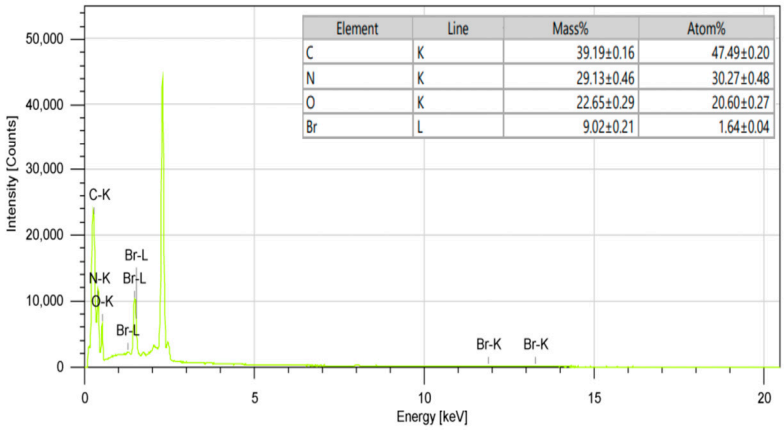

Preprints (www.preprints.org) | NOT PEER-REVIEWED | Posted: 25 December 2023 doi:10.20944/preprints202312.1792.v1

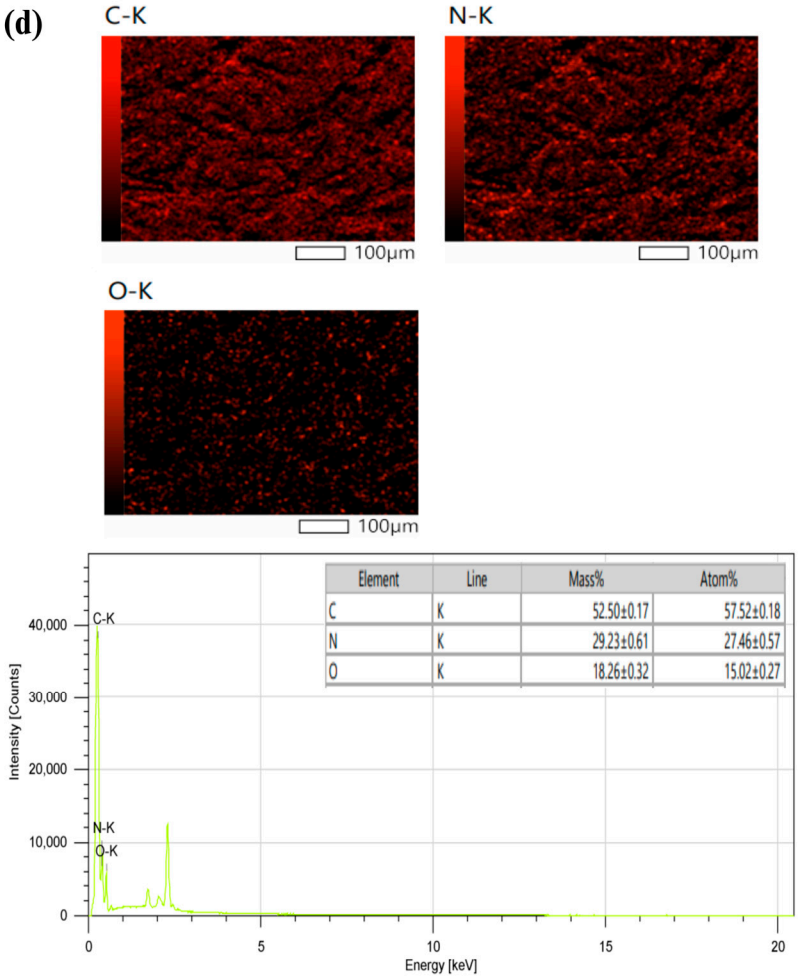

Figure 4. SEM images of (a) PAN-Br NA and (b) PAN-HNA at two µ magnification. EDX mapping analysis of (c) PAN-Br NA and (d) PAN-HNA.

A TGA study was utilized to determine the thermal stability of PAN-BrNA and PAN-HNA, as shown in Figure 5 (a, b), respectively. The networks of PAN-BrNA and PAN-HNA demonstrate a first degradation at temperatures 38-140 °C and 44-88 °C, with weight loss of 6% and 2.7%, respectively, caused by loss of solvent. PAN-BrNA exhibits main weight loss at temperatures of 140-412 °C. The thermogram shows that the polymer decomposes in three separate steps. In addition, the primary weight loss of PAN-HNA appeared at temperatures between 227-408 °C. The prior weight loss of the PANs owing to aminal linkage cleavage and the decomposition of triazine polymer networks begins at temperatures above 400 °C [20]. The polymer networks hold up their stability to 292 °C and 356 °C for PAN-BrNA and PAN-HNA, respectively.

Preprints (www.preprints.org) | NOT PEER-REVIEWED | Posted: 25 December 2023 doi:10.20944/preprints202312.1792.v1

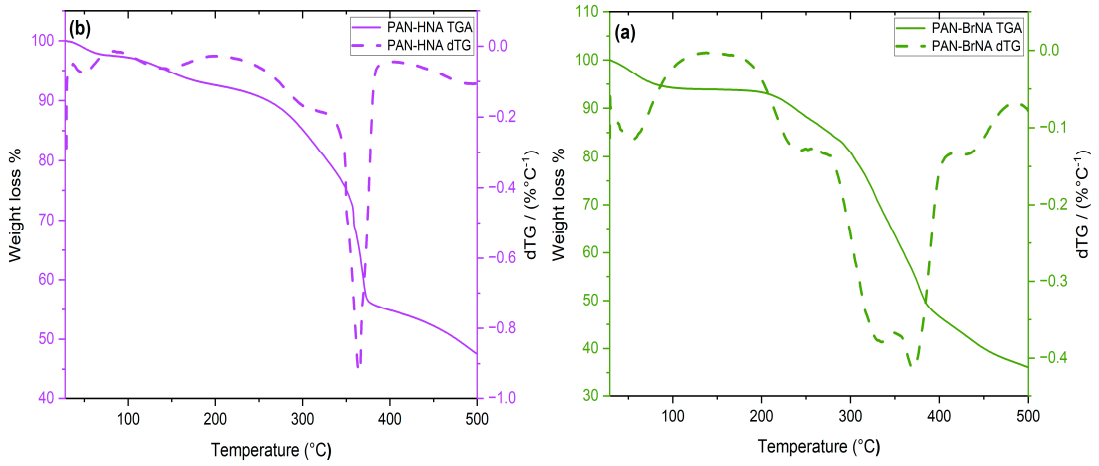

Figure 5. TGA (solid line) and dTG (dashed line) curves of (a) PAN-BrNA and (b) PAN-HNA.

Nitrogen sorption at 77 K was used to investigate the surface and porosity properties of PANs. As shown in Figure 6 (a), PAN-BrNA did not exhibit nitrogen adsorption, which implied the non-porous nature of the polymer networks as reported in previously synthesized PANs [18, 20]. As demonstrated in Figure 6 (b), PAN-HNA appears to contain mesopores that can be classified as type-IV isotherms; furthermore, PAN-HNA has an H2-type hysteresis loop related to more complicated pore structures and thin necks accompanied by broader bodies-ink bottle pores caused by pore-blocking/percolation in a narrow range of pore necks or cavitation-induced evaporation [21, 22]. A significant rise in nitrogen consumption in the ($P/P_0 < 0.01$) region of very low pressure indicates micropores in the structure. The values of BET surface area (S_{BET}), micropore surface area (S_{micro}), micropore volume (V_{micro}), and total pore volume (V_{total}) of the polyaminals are illustrated in Table 1. The Brunauer-Emmett-Teller (BET) surface area of PAN-BrNA is calculated to be 16.6990 m^2/g, and the total pore volume is 0.097320 cm^3/g. Figure 6 (c) depicts the calculated non-local density functional theory (NLDFT) pore size distribution, revealing that most pores in PAN-BrNA are 3.41 nm. The surface area and porous behavior of PAN-BrNA might be related to the bromine atoms, which occupy space and reduce the specific surface area along with the porous parameter [24]. PAN-HNA BET surface area has been determined to be 716.7568 m^2/g. The t-plot external surface area is 608.9677 m^2/g, demonstrating the occurrence of 107.7890 m^2/g microporous channels in the PAN-HNA structure. Figure 6 (d) depicts pore size distribution, showing that PAN-HNA pores are mainly distributed between 0.62 and 10.13 nm. In addition, PAN-HNA has a total pore volume of 0.729586 cm^3/g and a micropore volume of 0.042571 cm^3/g. The marked rise in surface area and decrease in porous parameters observed when compared to unfunctionalized PAN-NA previously reported could be attributed to the hydroxyl groups of PAN-HNA on the benzene occupying the partial pore space and the interactions between functional groups resulting in enhanced chain stacking [11, 19, 24].

Preprints (www.preprints.org) | NOT PEER-REVIEWED | Posted: 25 December 2023 doi:10.20944/preprints202312.1792.v1

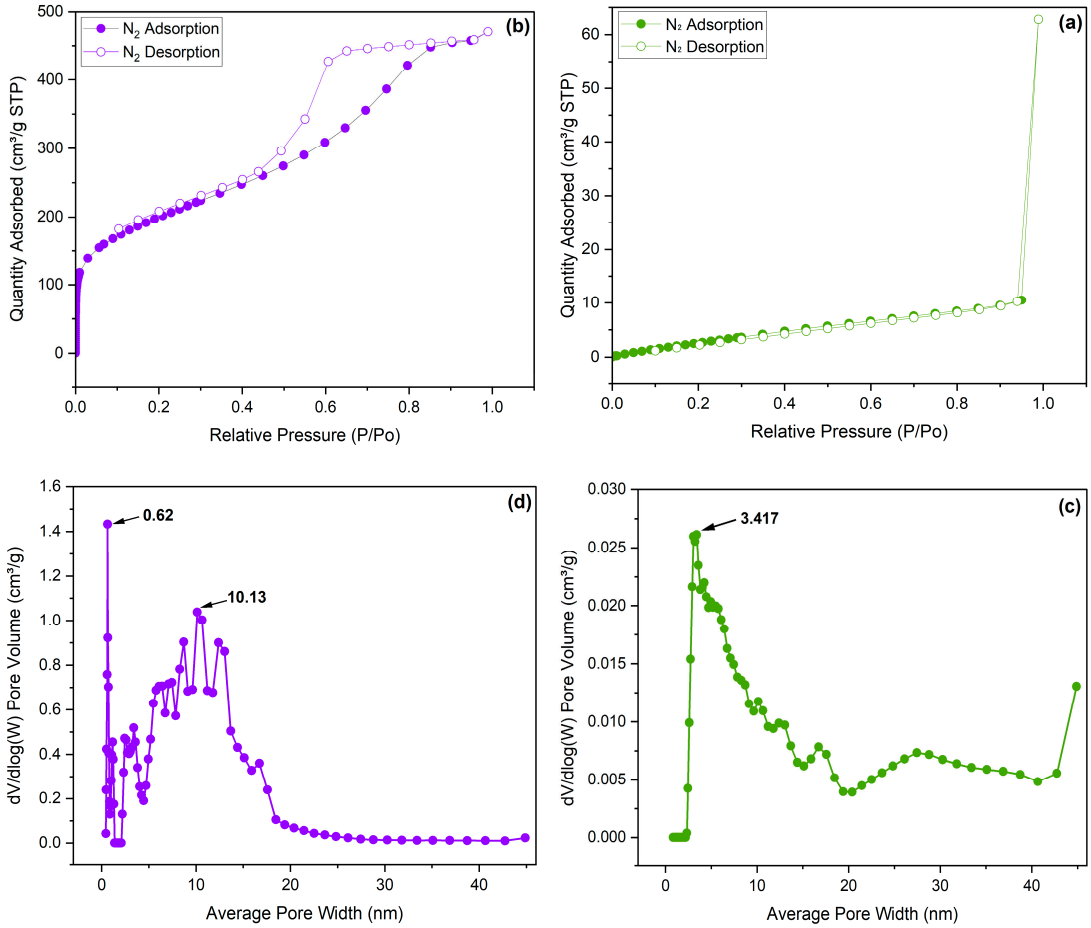

Figure 6. N_2 adsorption-desorption isotherm of (a) PAN-BrNA (b) PAN-HNA and pore size distribution calculated by NLDFT of (c) PAN-BrNA (d) PAN-HNA.

Table 1. Surface area and porosity parameters of PAN-BrNA and PAN-HNA polyaminals.

Sample	S_{BET} (m^2/g)	S_{micro} (m^2/g)	V_{micro} (cm^3/g)	V_{micro} (cm^3/g)
PAN-BrNA	16.699	0	0	0
PAN-HNA	716.757	107.789	0.04257	0.04257

3.2. CO_2 adsorption

The CO_2 isotherm at 273 K was determined up to 1 bar for measuring the CO_2 adsorption-desorption performance of both PANs, as demonstrated in Figure 7. PAN-BrNA CO_2 uptake was determined to be between 0.00628 and 4.42786 cm^3/g; similarly, PAN-HNA uptake ranged between 0.27256 and 47.55121 cm^3/g. The superior performance of melamine-based polymers could be attributed to the excellent interaction of polarizable CO_2 molecules with the polymer structure via dipole-quadrupole interactions and the constructed microporosity of polymers with a larger BET surface area [26]. For the reasons stated, PAN-HNA adsorbed more CO_2 than PAN-BrNA, which could be attributed to its larger surface area and the presence of substantial content of micropores, which increases the adsorption of small gas molecules. [21, 11]. The hydroxyl-functionalized PAN-HNA had a lower CO_2 adsorption than the previously reported unmodified PAN-NA, which had a higher uptake of up to 67.9 cm^3/g [25]. According to Zhang *et al.*, the hydroxyl-functionalized polymer MOP-1 has a lower CO_2 absorption than the unmodified polymer, and the low –OH content likely reduces CO_2 adsorption [27]. The noticeable hysteresis loops of CO_2 isotherms within PAN-BrNA and PAN-HNA suggested that chemical adsorption may occur along with physical adsorption. Table 2 compares the CO_2 adsorption of PAN-HNA to other reported hydroxyl-functionalized melamine-based polymers. PAN-HNA has a higher CO_2 uptake than MOP-1 and MOP-2 owing to its increased

Preprints (www.preprints.org) | NOT PEER-REVIEWED | Posted: 25 December 2023 doi:10.20944/preprints202312.1792.v1

surface area and microporosity content. Because of MOP-3 higher OH content, the dipolar or quadrupolar reaction between the oxygen atom of –OH and CO_2 molecules improved the polymer CO_2 capture capabilities [27]. The more extensive content of micropores in PAN-HP is beneficial for the adsorption of small gas molecules such as CO_2, resulting in enhanced CO_2 capture among all previously reported hydroxyl-functionalized melamine-based POPs [11].

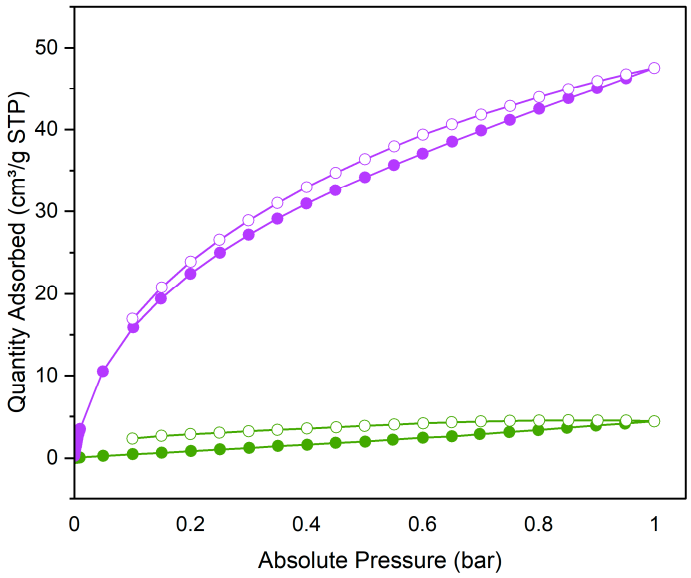

Figure 7. Adsorption (filled circles) and desorption (open circles) isotherms of CO_2 on PAN-BrNA (green) and PAN-HNA (violet) measured at 273 K up to 1 bar.

Table 2. The S_{BET} surface area and CO_2 absorption of diverse hydroxyl-functionalized melamine-based POPs.

Adsorbent	S_{BET} (m^2/g)	CO_2 Uptake at 1 bar (cm^3/g)	Ref.
		237 K	
PAN-HP	782	68.18	[11]
MOP-1	82	32.97	[27]
MOP-2	77	29.04	
MOP-3	36	57.77	
PAN-HNA	716.757	47.55	This work

4. Conclusions

New functionalized polyaminal-based polymers were synthesized via a one-pot polycondensation reaction. Melamine polymerizes with 2-bromo-1-naphthaldehyde and 2-hydroxy-1-naphthaldehyde to produce bromine and hydroxyl-functionalized hyper-cross-linked polymer networks PAN-BrNA and PAN-HNA, respectively. The PAN-BrNA, with a Brunauer-Emmett-Teller (BET) surface area of about (16.6990 m^2/g), can capture 4.42786 cm^3/g CO_2 gas. PAN-HNA has a higher BET surface area (716.7568 m^2/g) and micropores in the structure, resulting in a higher CO_2 capture (47.55121 cm^3/g). PAN-HNA networks exhibit notable promise in post-combustion CO_2 capture applications. Our findings demonstrate that functional groups can effectively adjust surface area and porosity characteristics, opening the possibility of further research into functionalized polyaminals networks.

References

1. A. Jaleel *et al.*, 'Hydrogenation of CO_2 to formates on ruthenium(III) coordinated on melamine polymer network', *J. CO_2 Util.*, vol. 35, pp. 245–255, Jan. 2020. https://doi.org/10.1016/j.jcou.2019.10.003.
2. Y. Hu *et al.*, 'New-Generation Anion-Pillared Metal–Organic Frameworks with Customized Cages for Highly Efficient CO_2 Capture', *Adv. Funct. Mater.*, vol. 33, no. 14, p. 2213915, Apr. 2023. https://doi.org/10.1002/adfm.202213915.
3. F. E. C. Othman, N. Yusof, and A. F. Ismail, 'Activated-Carbon Nanofibers/Graphene Nanocomposites and Their Adsorption Performance Towards Carbon Dioxide,' *Chem. Eng. Technol.*, vol. 43, no. 10, pp. 2023–2030, Oct. 2020. https://doi.org/10.1002/ceat.201900480.
4. M. Cavallo, M. Dosa, N. G. Porcaro, F. Bonino, M. Piumetti, and V. Crocellà, 'Shaped natural and synthetic zeolites for CO_2 capture in a wide temperature range', *J. CO_2 Util.*, vol. 67, p. 102335, Jan. 2023. https://doi.org/10.1016/j.jcou.2022.102335.
5. S. Yuan *et al.*, 'Triazine-functionalized highly ordered hierarchically porous organic polymer with high CO_2 uptake capacity and catalytic activity for microwave-assisted Knoevenagel condensation reaction', *Colloids Surf. Physicochem. Eng. Asp.*, vol. 607, p. 125475, Dec. 2020. https://doi.org/10.1016/j.colsurfa.2020.125475.
6. K. S. Song, P. W. Fritz, and A. Coskun, 'Porous organic polymers for CO_2 capture, separation and conversion', *Chem. Soc. Rev.*, vol. 51, no. 23, pp. 9831–9852, 2022. https://doi.org/10.1039/D2CS00727D.
7. W. Wang, M. Zhou, and D. Yuan, 'Carbon dioxide capture in amorphous porous organic polymers,' *J. Mater. Chem. A*, vol. 5, no. 4, pp. 1334–1347, 2017. https://doi.org/10.1039/C6TA09234A.
8. G. Li, B. Zhang, and Z. Wang, 'Facile Synthesis of Fluorinated Microporous Polyaminals for Adsorption of Carbon Dioxide and Selectivities over Nitrogen and Methane,' *Macromolecules*, vol. 49, no. 7, pp. 2575–2581, Apr. 2016. https://doi.org/10.1021/acs.macromol.6b00147.
9. Z. Xiang *et al.*, 'Systematic Tuning and Multifunctionalization of Covalent Organic Polymers for Enhanced Carbon Capture,' *J. Am. Chem. Soc.*, vol. 137, no. 41, pp. 13301–13307, Oct. 2015. https://doi.org/10.1021/jacs.5b06266.
10. R. Dawson, D. J. Adams, and A. I. Cooper, 'Chemical tuning of CO_2 sorption in robust nanoporous organic polymers', *Chem. Sci.*, vol. 2, no. 6, p. 1173, 2011. https://doi.org/10.1039/c1sc00100k.
11. B. Zhang, J. Yan, G. Li, and Z. Wang, 'Carboxyl-, Hydroxyl-, and Nitro-Functionalized Porous Polyaminals for Highly Selective CO_2 Capture', *ACS Appl. Polym. Mater.*, vol. 1, no. 6, pp. 1524–1531, Jun. 2019. https://doi.org/10.1021/acsapm.9b00297.
12. P. M. C. Matias, D. Murtinho, and A. J. M. Valente, 'Triazine-Based Porous Organic Polymers: Synthesis and Application in Dye Adsorption and Catalysis,' Polymers, vol. 15, no. 8, p. 1815, Apr. 2023. https://doi.org/10.3390/polym15081815.
13. B. Zhang, J. Yan, Y. Shang, and Z. Wang, 'Synthesis of Fluorescent Micro- and Mesoporous Polyaminals for Detection of Toxic Pesticides,' *Macromolecules*, vol. 51, no. 5, pp. 1769–1776, Mar. 2018. https://doi.org/10.1021/acs.macromol.7b02669.
14. S. Zappia *et al.*, 'Microporous Polymelamine Framework Functionalized with Re(I) Tricarbonyl Complexes for CO_2 Absorption and Reduction', *Polymers*, vol. 14, no. 24, p. 5472, Dec. 2022. https://doi.org/10.3390/polym14245472.
15. H. Li, C. Li, J. Chen, L. Liu, and Q. Yang, 'Synthesis of a Pyridine-Zinc-Based Porous Organic Polymer for the Co-catalyst-Free Cycloaddition of Epoxides,' *Chem. - Asian J.*, vol. 12, no. 10, pp. 1095–1103, May 2017. https://doi.org/10.1002/asia.201700258.
16. Z. Li, Y. Zhi, Y. Ni, H. Su, Y. Miao, and S. Shan, 'Novel melamine-based porous organic materials as metal-free catalysts for copolymerization of SO_2 with epoxide', *Polymer*, vol. 217, p. 123434, Mar. 2021. https://doi.org/10.1016/j.polymer.2021.123434.
17. R. A. El-Ghazawy *et al.*, 'Preparation and characterization of melamine-based porous Schiff base polymer networks for hydrogen storage,' *J. Polym. Res.*, vol. 21, no. 6, p. 480, Jun. 2014. https://doi.org/10.1007/s10965-014-0480-x.
18. C. Liu *et al.*, 'One-pot synthesis of nitrogen-rich aminal- and triazine-based hierarchical porous organic polymers with highly efficient iodine adsorption,' *Polymer*, vol. 194, p. 122401, Apr. 2020. https://doi.org/10.1016/j.polymer.2020.122401.
19. R. Sandín, M. González-Lucas, P. A. Sobarzo, C. A. Terraza, and E. M. Maya, 'Microwave-assisted melamine-based polyaminals and their application for metal cations adsorption,' *Eur. Polym. J.*, vol. 155, p. 110562, Jul. 2021. https://doi.org/10.1016/j.eurpolymj.2021.110562.
20. K. Yuan *et al.*, 'Facile synthesis and study of functional porous organic polyaminals with ultrahigh adsorption capacities and fast removal rate for rhodamine B dye,' *Microporous Mesoporous Mater.*, vol. 344, p. 112234, Oct. 2022. https://doi.org/10.1016/j.micromeso.2022.112234.
21. P. A. Sobarzo, A. Tundidor, E. S. Sanz-Perez, C. A. Terraza, and E. M. Maya, 'Effect of thiophene, furan moieties and zinc ions on melamine-based porous polyaminals properties and catalytic activity on CO_2 cycloaddition reaction', *Eur. Polym. J.*, vol. 177, p. 111444, Aug. 2022. https://doi.org/10.1016/j.eurpolymj.2022.111444.

22. R. Bardestani, G. S. Patience, and S. Kaliaguine, 'Experimental methods in chemical engineering: specific surface area and pore size distribution measurements—BET, BJH, and DFT,' *Can. J. Chem. Eng.*, vol. 97, no. 11, pp. 2781–2791, Nov. 2019. https://doi.org/10.1002/cjce.23632.
23. A. O. Mousa, M. G. Mohamed, C.-H. Chuang, and S.-W. Kuo, 'Carbonized Aminal-Linked Porous Organic Polymers Containing Pyrene and Triazine Units for Gas Uptake and Energy Storage,' *Polymers*, vol. 15, no. 8, p. 1891, Apr. 2023. https://doi.org/10.3390/polym15081891.
24. E. S. Sanz-Pérez, L. Rodríguez-Jardón, A. Arencibia, R. Sanz, M. Iglesias, and E. M. Maya, 'Bromine pre-functionalized porous polyphenylenes: New platforms for one-step grafting and applications in reversible CO_2 capture', *J. CO_2 Util.*, vol. 30, pp. 183–192, Mar. 2019. https://doi.org/10.1016/j.jcou.2019.02.005.
25. M. Ibrahim, N. Tashkandi, N. Hadjichristidis, and N. S. Alkayal, 'Synthesis of Naphthalene-Based Polyaminal-Linked Porous Polymers for Highly Effective Uptake of CO_2 and Heavy Metals', *Polymers*, vol. 14, no. 6, p. 1136, Mar. 2022. https://doi.org/10.3390/polym14061136.
26. F. Tang, J. Hou, K. Liang, J. Huang, and Y. Liu, 'Melamine-Based Metal-Chelating Porous Organic Polymers for Efficient CO_2 Capture and Conversion', *Eur. J. Inorg. Chem.*, vol. 2018, no. 37, pp. 4175–4180, Oct. 2018. https://doi.org/10.1002/ejic.201800764.
27. N. Zhang, B. Zou, G.-P. Yang, B. Yu, and C.-W. Hu, 'Melamine-based mesoporous organic polymers as metal-Free heterogeneous catalyst: Effect of hydroxyl on CO_2 capture and conversion', *J. CO_2 Util.*, vol. 22, pp. 9–14, Dec. 2017. https://doi.org/10.1016/j.jcou.2017.09.001.